Cities 131 (2022) 103988

Contents lists available at ScienceDirect

Cities

journal homepage: www.elsevier.com/locate/cities

The characteristic and transformation of 3D urban morphology in three Chinese mega-cities

Zhi Cai [a], Matthias Demuzere [b], Yan Tang [a,*], Yongman Wan [a]

[a] School of Architecture, Tsinghua University, Beijing 100084, China
[b] Urban Climatology Group, Department of Geography, Ruhr-University Bochum, Bochum, Germany

ARTICLE INFO

Keywords:
Urban morphology
Local climate zone
Transformation
Driving forces
3D
Machine learning

ABSTRACT

Urban morphology exerts an important influence on human settlements and serves to promote sustainable development. However, few studies have focused on the three dimensions (3D) of urban morphology. Therefore, to explore 3D urban morphological characteristics and transformations, we adopted a standard urban morphology classification scheme, the local climate zone (LCZ), and selected three Chinese megacities as case studies. Remote sensing images and machine-learning technology were used to create spatiotemporal LCZ maps. Our results reveal that cities have diverse forms, with the dominant urban morphology varying across different cities and periods. However, cities still share several common patterns. The dynamic spatial distribution of LCZ density can be divided into three patterns: spreading, shrinking and relocation. In recent years, Chinese mega-cities have mainly expanded with open high-rise (OHR) and large low-rise (LLR) classes. Combined with the increase in building height, urban landscapes have been homogeneous. Additionally, 3D urban morphology is driven by several factors, such as economic activity and the dissociation of population growth from urban expansion. Detailed spatiotemporal LCZ maps can help us better understand urban morphology transformations and explore the corresponding driving forces, providing a reference for urban planners and policymakers seeking to make cities healthier and more livable.

1. Introduction

Urban morphology refers to the physical characteristics of urban forms, such as the spatial layout of buildings, the urban landscape and its transformations (Chen, 2014). As a product of human construction and a reflection of urban function, urban morphologies changes with development. An inappropriate urban morphology can accelerate microclimate change, threaten human health, impact the urban environment and other issues (Cai, Han, & Chen, 2018; Cao, Luan, Liu, & Wang, 2021; Cao, Wu, Liu, Chen, & Zou, 2019; Milojevic-DuPont & Creutzig, 2020). Scholars have also found that planning strategies used to optimize the physical urban morphology are an efficient way to address the above noted issues through urban design (Hatvani-Kovacs, Bush, Sharifi, & Boland, 2018; Mabon, Kondo, Kanekiyo, Hayabuchi, & Yamaguchi, 2019). Therefore, to promote sustainable urban development, there is an urgent need to explore the characteristics of urban morphology and reveal the driving forces behind corresponding transformations.

Classic urban morphology studies were usually conducted in two dimensions (2D) and discussed various issues, such as land use, urban structure, and the driving forces behind morphological transformation (Kovács et al., 2019; Li, Sun, & Fang, 2018; Meng, Sun, & Zhao, 2020; Yang, Zhang, Xu, & Luo, 2020). In land use studies, remote sensing techniques combined with geographic information system (GIS) methods have been widely applied to capture urban morphology characteristics by using satellite data (e.g., Landsat series images and nighttime light images) (Taubenböck et al., 2012; Zhang & Seto, 2011). Land use is typically classified into natural land and built-up areas, whereby the boundaries and locations of built-up areas are regarded as crucial factors in the evaluation of urban morphology dynamics, such as outlying expansion and infilling (He, Zeng, Xie, Tan, & Wu, 2019; Yang et al., 2020; Zhao et al., 2020). While focusing on built-up areas and urban boundaries, scholars have also used landscape metrics (e.g., area, shape, and density) to quantify and explore the dynamics of urban morphology at the mesoscale (Lemoine-Rodríguez, Inostroza, & Zepp, 2020; Meng et al., 2020; Wentz et al., 2018; Yu & Ng, 2007). For example, Meng et al. (2020) used landscape metrics to compare the spatiotemporal dynamics of urban expansion in Guangzhou and Shenzhen, they found that both cities exhibited leapfrogging growth

* Corresponding author.
E-mail addresses: czhi0911@gmail.com (Z. Cai), matthias.demuzere@rub.de (M. Demuzere), yantang@mail.tsinghua.edu.cn (Y. Tang).

https://doi.org/10.1016/j.cities.2022.103988
Received 20 July 2021; Received in revised form 12 September 2022; Accepted 15 September 2022
Available online 28 September 2022
0264-2751/© 2022 Elsevier Ltd. All rights reserved.

followed by edge expansion. Lemoine-Rodríguez et al. (2020) compared the dynamics of 194 cities across the globe using landscape metrics and found that large cities tend toward fragmentation, while small cities have become increasingly compact. Previous studies have also revealed that the transformation of urban morphology is driven by multiple factors, such as government policy, socioeconomic development, and natural resources (Li et al., 2018; Long, Gu, & Han, 2012; Wu, Li, & Wang, 2021; Yang et al., 2020).

In addition to 2D-level urban morphology studies, in recent years, 3D-level studies have rapidly increased in popularity with the enrichment of data sources (e.g., OpenStreetMap and Google Earth 3D layers), and the development of optical or stereo remote sensing technology (Fonte, Lopes, See, & Bechtel, 2019; Taubenböck, Standfuß, Wurm, Krehl, & Siedentop, 2017; Xu et al., 2017; Zhu et al., 2019). Several parameters are widely applied to illustrate 3D urban morphology characteristics, such as the street aspect ratio, building height, built-up volume and sky view factor (Biljecki & Ito, 2021; Cao et al., 2019; Li, Liu, Zhang, Xue, & Li, 2021; Taubenböck et al., 2017). For example, Taubenböck et al. (2017) used stereoscopic remote sensing images in combination with building footprint data to derive urban 3D building models and then applied a built-up volume parameter to analyze urban mass concentrations. Researchers have also proposed some schemes to systematically classify urban morphology, such as urban functional zones and local climate zones (LCZ) (Du, Liu, & Zhang, 2021; Stewart & Oke, 2012). In particular, the LCZ scheme is rapidly gaining attention in this field (Jiang et al., 2021). The scheme was adopted by the World Urban Database and Access Portal Tool (WUDAPT) community project (Ching et al., 2018), in which the lowest level of detail was used to map cities and their surrounding natural landscapes into LCZ types. Combined with characteristic urban canopy parameters, the LCZ scheme also provides information on urban physical forms and functions in global cities in a standardized manner. At present, LCZ have been widely applied in urban climate studies (Demuzere, Kittner, & Bechtel, 2021) and have been expanded for use in other applications, such as human health, socioeconomic and urban morphology analyses (Brousse et al., 2019; Cai, Tang, Chen, & Han, 2019; Cai, Tang, & Zhan, 2021; Ren et al., 2019; Taubenböck et al., 2020). Scholars have also constructed dynamic LCZ maps for different cities (Demuzere, Mihara, Redivo, Feddema, & Setton, 2020; Vandamme, Demuzere, Verdonck, Zhang, & Van Coillie, 2019; Wang et al., 2019; Zhao, Weng, & Hersperger, 2020). For example, Vandamme et al. (2019) quantified the expansion and intra-urban restructuring of Kunming from 2005 to 2017 based on LCZ and found that Kunming city experienced spatial expansion between 2005 and 2011, whereas densification with open classes commenced after 2011. Zhao et al. (2020a) characterized the urban morphology of Austin, TX (USA), analyzed its transformation between 2006 and 2016 based on an improved LCZ classification scheme and found that the city mainly expanded with sparsely built and transportation classes.

However, previous 2D and 3D urban morphology studies suffered from certain limitations. For example, 2D studies can illustrate urban expansion characteristics well, but they neglect parts of the urban morphology that can be addressed based on its 3D characteristics, such as building height and volume. Moreover, 2D studies have difficulty capturing urban renewal characteristics in built-up areas in which urban renewal has become a dominant phenomenon in developed cities or regions with limited expansion (Carmon, 1999). Early 3D studies were usually conducted at the microscale because of the lack of freely available data at the mesoscale. In recent years, professional services (e.g., Geoscape and Baidu Map) have begun to provide fine-scale spatial 3D urban products (Li, Koks, Taubenböck, & van Vliet, 2020; Potgieter et al., 2021); however, such datasets are expensive, and most span only a specific period in time. Such shortcomings have limited the study of 3D urban morphology transformations and comparisons across different cities worldwide. Furthermore, previous studies of LCZ dynamics mainly focused on urban expansion characteristics and only addressed urban renewal in a limited way. Whether cities display a similar pattern in terms of spatial layout transformation and the characterization of 3D urban morphology remains unknown. Moreover, most studies have been limited to revealing the forces driving the 3D urban morphology.

In recent years, machine learning, especially deep-learning technology, has experienced rapid development in natural language processing, data mining, multimedia learning and other areas (LeCun, Bengio, & Hinton, 2015). In particular, image recognition technology based on convolutional neural networks and random forests has accelerated urban studies (Grekousis, 2019; Li et al., 2019). The fusion of free multisource satellite data combined with machine/deep learning, remote sensing technology and GIS has made it possible to quickly identify and classify 3D urban morphology at a high spatiotemporal resolution worldwide (Geiß, Schrade, Pelizari, & Taubenböck, 2020; Ma et al., 2019; Middel, Nazarian, Demuzere, & Bechtel, 2022; Yu, Wu, Luo, & Ren, 2017). Therefore, in this paper, we adopted machine learning, remote sensing and the LCZ scheme to answer the following questions:

1) What characteristics of 3D urban morphology have been transformed across different cities?
2) What are the main forces driving 3D urban morphology transformations?

2. Data and methods

2.1. Case study cities

Over the past 20 years, China has experienced rapid urbanization, with the area of built-up urban land increasing from 22,439 km^2 to 60,312 km^2, simultaneously increasing the permanent urban population from 30.89 % to 60.6 % of the total population (NBS, 2020). Moreover, China has a vast territory with varied landscapes and diverse cultures, leading to diverse 3D urban morphology characteristics across different cities. Therefore, three Chinese megacities were selected as case studies: Beijing, Shanghai and Guangzhou (Fig. 1). Beijing, long China's capital, has a historical urban core area that dates back 600 years (Gaubatz, 1995). Because of the city's numerous historical conservation zones, dense population, and scarce water resources, top-down central government policies heavily influence urban planning and construction (Long et al., 2012; Wu, 2015). Shanghai, the economic center of China, is one of the largest trade port cities to emerge in the modern period; its traditional urban landscape was influenced by Western cultures in the early 20th century (Lee & Li, 1999). Guangzhou, at the center of the Pearl River Delta, was China's first national pioneering urbanization area beginning in 1978, and as a result, market forces have been a stronger driver of urban development there than in other Chinese cities (Yu & Ng, 2007). Beijing, Shanghai, and Guangzhou represent three typical Chinese cities of the 20th century: traditional, modern and socialist (Gaubatz, 1999). They also have similarities. For example, they are located in the country's three largest urban agglomerations (the Jing-Jin-Ji, Yangtze-River-Delta and Pearl-River-Delta urban agglomerations) (Fig. 1), and they are densely populated, with 21.54 million, 24.28 million and 15.3 million residents, respectively. All have experienced rapid urbanization and large urban morphology transformations over the past two decades. Therefore, Beijing, Shanghai, and Guangzhou are ideal megacities for a comparative study that aims to identify and reveal the driving forces behind 3D urban morphology transformations.

2.2. Data sources and preprocessing

To conduct a long-term series of studies, we chose Landsat satellite series data (e.g., Landsat 5, 7+ and 8) for urban morphology classification because they have been freely available since 1984. The spatial resolution of Landsat satellite images ranges from 15 m to 120 m, and it is difficult to identify the fine-scale characteristics (e.g., building footprints and small rivers) of the urban morphology at those resolutions. To overcome this problem, we selected Google historical images with a



Fig. 1. Locations of the case cities and study area.

super high spatial resolution (1 m) as a label layer and Landsat imagery as Earth observation input features. Google historical data were extracted from Google Earth, and Landsat imagery was accessed from the Google Earth Engine (GEE) platform. Population density data at a spatial resolution of 1 km were downloaded from the WorldPop website (https://www.worldpop.org/) and resampled to a 100 m resolution to fit urban morphology maps. Population size data were acquired from the report of Demographia World Urban Areas (Cox, 2021). Gross domestic product (GDP) data for global megacities were acquired from the World Bank website (https://data.worldbank.org/).

2.3. Methods

2.3.1. Classification of 3D urban morphology and accuracy assessment

We adopted an adapted LCZ scheme to classify the 3D urban morphology (Fig. 2). LCZ classified urban and rural areas into built-up (LCZ 1 to 10) and natural land cover (LCZ A to G) categories with 17 different classes (Stewart & Oke, 2012) (Table 1A, Appendix). Because the LCZ scheme was mainly designed for urban climate studies, certain LCZ classes have similar functions and can be regarded as the same type in urban planning. For example, dense trees (LCZ A), scattered trees

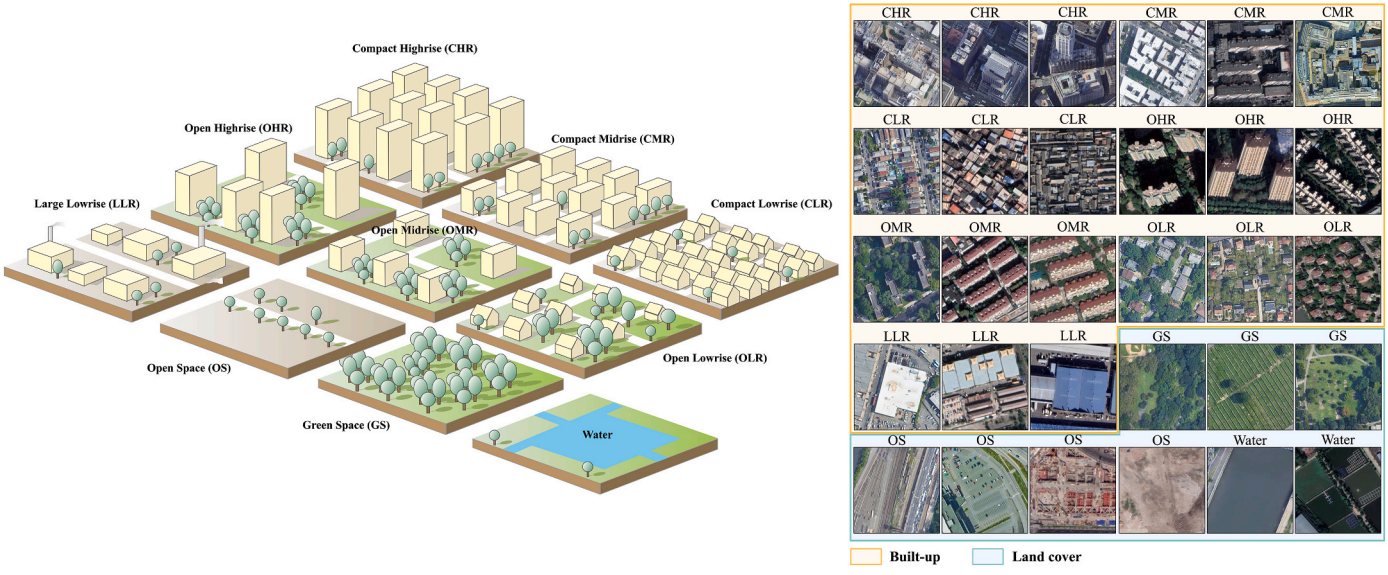


Fig. 2. Adapted LCZ scheme applied in our study and the corresponding labeled samples.

(LCZ B), bush and scrub (LCZ C), and low plants (LCZ D) are all considered green spaces in urban planning. The large low-rise (LLR, LCZ 8) and heavy industry (LCZ 10) classes are mainly associated with industrial functions. Therefore, we deleted and merged several LCZ classes to make them suitable for urban morphology studies as follows. LCZ A-D were reclassified into green space (GS), and LCZ E-F were reclassified into open space (OS). LCZ 8 and LCZ 10 were merged into LLR. Specifically, compact high-rise (CHR), compact mid-rise (CMR), compact low-rise (CLR), open high-rise (OHR), open mid-rise (OMR), open low-rise (OLR) and LLR are built-up classes. Additionally, GS, OS and water are natural land cover classes.

Multitemporal LCZ maps were created using the historical Google layers and Earth observation input features from the Landsat satellite images (Fig. 3). First, we imported the available Google historical layers into ArcGIS Pro software. Then, we digitized the labeled training areas (TAs) required for the supervised random forest classifier (Bechtel et al., 2015). Because of the super-high-resolution Google historical layers are available only after 2000, and the processes of urban demolition and reconstruction can last several years. Therefore, the year 2000 was selected as a starting point, with additional target years selected 5 years apart (2000, 2005, 2010, 2015 and 2020). For all target years, all Landsat images within ±180 days were selected (e.g., 01-07-1999 to 01-07-2001 for the year 2000), and only data obtained on days with cloud cover below 70 % were used. The total numbers of labeled training area polygons for Beijing, Shanghai and Guangzhou were 11,705, 13,059, and 10,599, respectively. These labels were uploaded to the GEE to perform the LCZ classification using GEE resources according to the approach of Demuzere (Demuzere et al., 2020; Demuzere et al., 2021; Demuzere, Bechtel, Middel, & Mills, 2019; Demuzere, Bechtel, & Mills, 2019). The classification procedure generally followed the methodology used in the LCZ generator (http://lcz-generator.rub.de, Demuzere et al., 2021), with certain changes to the Earth observation input features because of the multitemporal nature of the classification problem.

The accuracy assessment followed the standard cross-validation approach (Bechtel et al., 2019; Demuzere et al., 2021): in each of the 25 bootstraps, 70 % of the TA polygons were used for training, and 30 % were used for testing. The polygons were selected by stratified (LCZ type) random sampling, maintaining the original LCZ class frequency distribution. This procedure was repeated 25 times, which enabled us to provide confidence intervals for the accuracy metrics. The accuracy metrics included the overall accuracy (OA), overall accuracy for the urban LCZ classes only (OA_u), overall accuracy of the built vs. natural LCZ classes only (OA_{bu}), and weighted accuracy (OA_w). For further details, see the studies of Bechtel, Demuzere, and Stewart (2020) and Demuzere et al. (2021).

2.3.2. Spatial unit and distribution of urban morphology

The spatial unit is a fundamental parameter that influences the detailed description of urban morphologies. To utilize the minimum scale (100 m) in the proposed LCZ scheme, we selected 100 m × 100 m grid cells as the spatial unit to map and analyze the data.

We applied ring-based analysis to capture the natural continuous spatial distribution of the 3D urban morphology, a method widely used in previous 2D urban morphology studies (Jiao, 2015; Xu et al., 2019). This approach aims to prevent the morphological characteristics from being influenced by changes in urban/administrative boundaries, and can be used to easily identify matching areas and compare different cities. In the ring-based method, the central business district (CBD) is set as the city center, and a series of buffer zones is then established around it. As the location of the CBD may change over time, we fixed this location to a site identified in the 1990s. Although ring-based methods are mainly used for monocentric cities, they can also be applied in polycentric regions. The difference is that the latter have multiple city centers. In previous studies (Jiao, 2015), the effective radius in most Chinese cities is < 36 km; therefore, to capture most of the built-up classes in all periods, the longest distance from the city center to the outside buffer zones was 36 km for all cities, and the width of buffer zones was set as 1 km (Fig. 4a). The spatial distribution of the LCZ classes can be described by their density in each buffer zone and expressed as follows:

$$D_{cj}^{i} = \frac{CA_j}{TA_j}\left(i = 2000,\ 2005\ldots2020;\ j = 1,\ 2\ldots36\right) \quad (1)$$

where D is density; C represents the different LCZ classes (e.g., CHR, CMR, and OLR); j is the buffer zone; CA_j is the area of class C in the j^{th} ring; TA_j represents the total area of the j^{th} ring; and i is the year. Therefore, D_{CHR1}^{2000} is the density of the CHR class in the 1st buffer zone in 2000. To clearly show the spatial distribution of the LCZ classes, we performed spline fitting between each LCZ density class and the corresponding distance to the city center (DIST).

2.3.3. Alluvial diagram model

Exploring the transformation of different LCZ classes is crucial for understanding urban development and its driving forces. Previously, 2D studies typically addressed urban expansion in terms of several subcategories, such as edge expansion and outlying (He et al., 2019; Meng et al., 2020; Zhang et al., 2020), but few of them accounted for urban renewal. Therefore, to capture all types of urban morphological dynamics, we classified them into two categories: expansion and renewal. Expansion involves the replacement of natural land cover classes (e.g., GS, OS, and water) with built-up classes (e.g., CHR, CMR, and LLR); in contrast, renewal represents a built-up class that changes and is replaced by another built-up class (or natural land cover class) across different periods (Fig. 4a). An alluvial diagram was also used to illustrate the LCZ class transformations in fixed study areas (Fig. 4b). Additional details regarding alluvial diagrams were provided by Rosvall and Bergstrom (2010).

3. Results

3.1. Classification accuracy

Most of the LCZ classifications achieved OA scores well above 0.6 (Fig. 5), thus meeting the average minimum accuracy (0.5) requirement for WUDAPT automated quality control (Bechtel et al., 2019), which demonstrating that the classified results are reliable and can be used in subsequent spatial analyses. The average OA_{bu} in all cities and periods was > 0.9, which indicates that built-up areas and natural land covers were well classified. Similarly, all of the OA_w values reached average

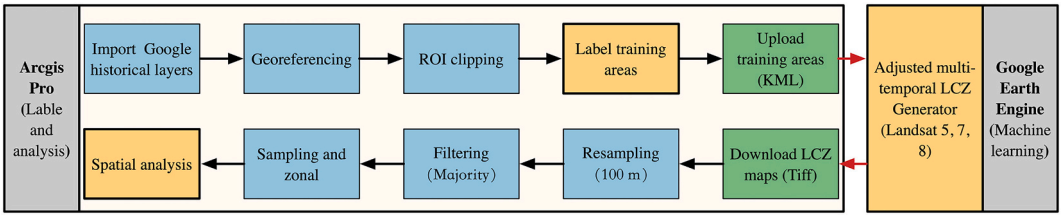


Fig. 3. Workflow of urban morphology classification and spatial analysis.

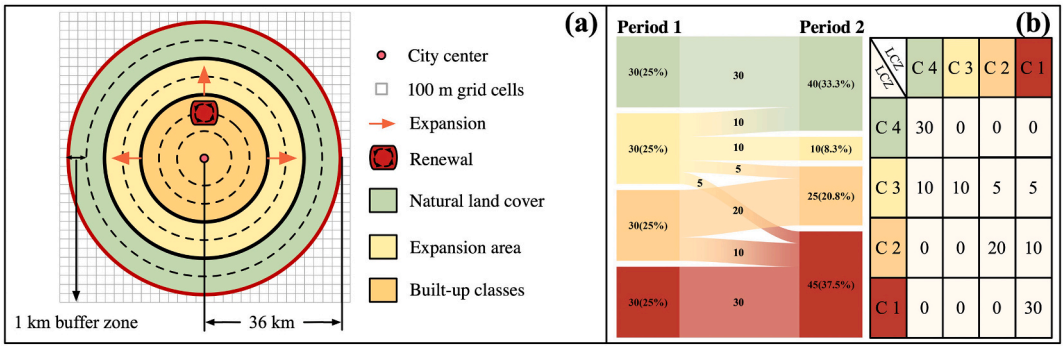


Fig. 4. Conceptual illustration of the ring-based method (a), an alluvial diagram model and the corresponding transition matrix (b). In the latter, C1, C2, C3 and C4 represent different LCZ classes.

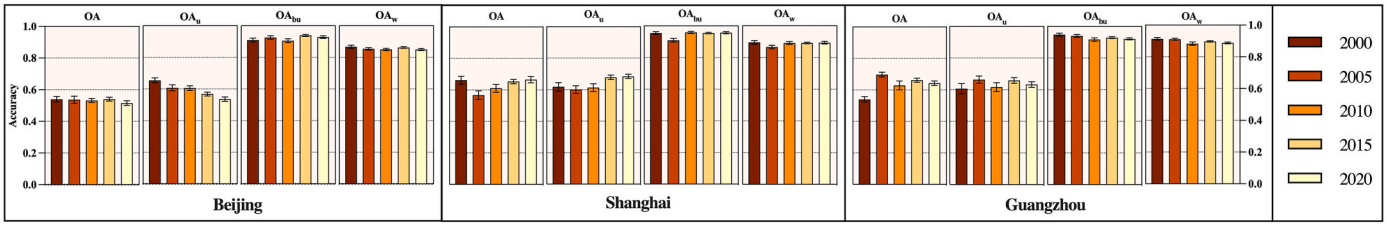


Fig. 5. Accuracy metrics across three cities and different years.

values > 0.85, which indicates that the dissimilarity between LCZ types (e.g., compact and open classes) was well recognized.

3.2. 3D urban morphology characteristics

Cities are unique in their landscape and physical characteristics. However, cities are also typically composed of the same elements, such as buildings, roads and green spaces, and those elements form different urban morphology classes. Therefore, uniqueness and universality exist simultaneously. To explore these dual characteristics of cities, we perform assessments from the perspectives of dominant urban morphology classes and spatial distributions.

3.2.1. Dominant urban morphology classes across different cities

Although the dominant LCZ classes varied across different cities, there was a common trend of these classes transforming to high-rise classes (Fig. 6). In their early stages, the studied cities mainly consisted of low-rise or mid-rise buildings; notably, in 2000, the dominant built-up classes in Beijing, Shanghai and Guangzhou were CLR, OMR and LLR, accounting for 57.2 %, 45.7 % and 24 % of the built-up areas, respectively. Later, especially after 2010, the number of high-rise buildings in urban built-up areas quickly increased. For example, the percentage of the OHR class in the study area increased from 0.2 % (2000) to 8 % (2020) in Beijing, from 2.1 % (2000) to 34.5 % (2020) in Shanghai, and from 0.1 % (2000) to 9.2 % (2020) in Guangzhou.

3.2.2. Spatial distribution of 3D urban morphology

The distribution of LCZ classes revealed a spatial preference. For example, compact classes (e.g., CHR and CMR) were concentrated in urban core areas, while LLR classes were located in outer rings. For the CHR and CMR classes, most appeared in urban core areas with DIST values < 10 km. However, CHR and CMR exhibited contrasting development models, as the number of CHR increased while CMR in abundance decreased with urban development (Fig. 7). The density of the CLR class also exhibited a decreasing trend for all cities in urban core areas. LLR were most likely to appear in suburban areas with DIST values > 10 km. Notably, the LLR density decreased near urban core areas but increased in suburban areas with urban development. The OHR class was more likely to appear in areas with DIST values > 10 km, and the density of this class increased in both urban core areas and suburban areas. The OMR class tended to appear in areas with DIST values ranging from 10 km to 20 km and displayed the highest density value in these areas.

From Fig. 7, we can categorize the development and spatial distribution of LCZ classes into three fundamental patterns: spreading, shrinking, and relocation (Fig. 8). Spreading occurs when the density and area of an LCZ class increase (Fig. 8a); this pattern was common for the CHR and OHR classes. Shrinking occurs when the density and area of an LCZ class decrease (Fig. 8b); this pattern was most common for the CLR class. Relocation is associated with a constant LCZ density. However, the location of a class shifts from one area to other areas in the course of urban development (Fig. 8c). Relocation was most common for the LLR classes. The three fundamental patterns can also be applied to multiple types of distribution. For example, the development of the CMR class in Beijing involved shrinking and spreading (Fig. 7a-2).

3.3. Transformation of 3D urban morphology

From the perspective of urban development, morphological transformations can be divided into two types: expansion and renewal. Because of rapid urbanization, outward expansion was the major phenomenon witnessed in most Chinese cities in the early phase, especially before 2010. After 2010, affected by the declines in economic growth and the urbanization speed, urban expansion slowed, and the percentage of internal urban renewal in built-up areas gradually increased (Fig. 9).

3.3.1. Characterization of urban expansion

Expansion was a popular trend of urbanization, with the built-up area increasing by 6.5 %, 42.2 %, and 29.2 % in Beijing, Shanghai and Guangzhou, respectively, between 2000 and 2020. The fastest expansion appeared in approximately 2010, after which it gradually slowed in all cities.

A detailed examination of the transformation of LCZ classes showed

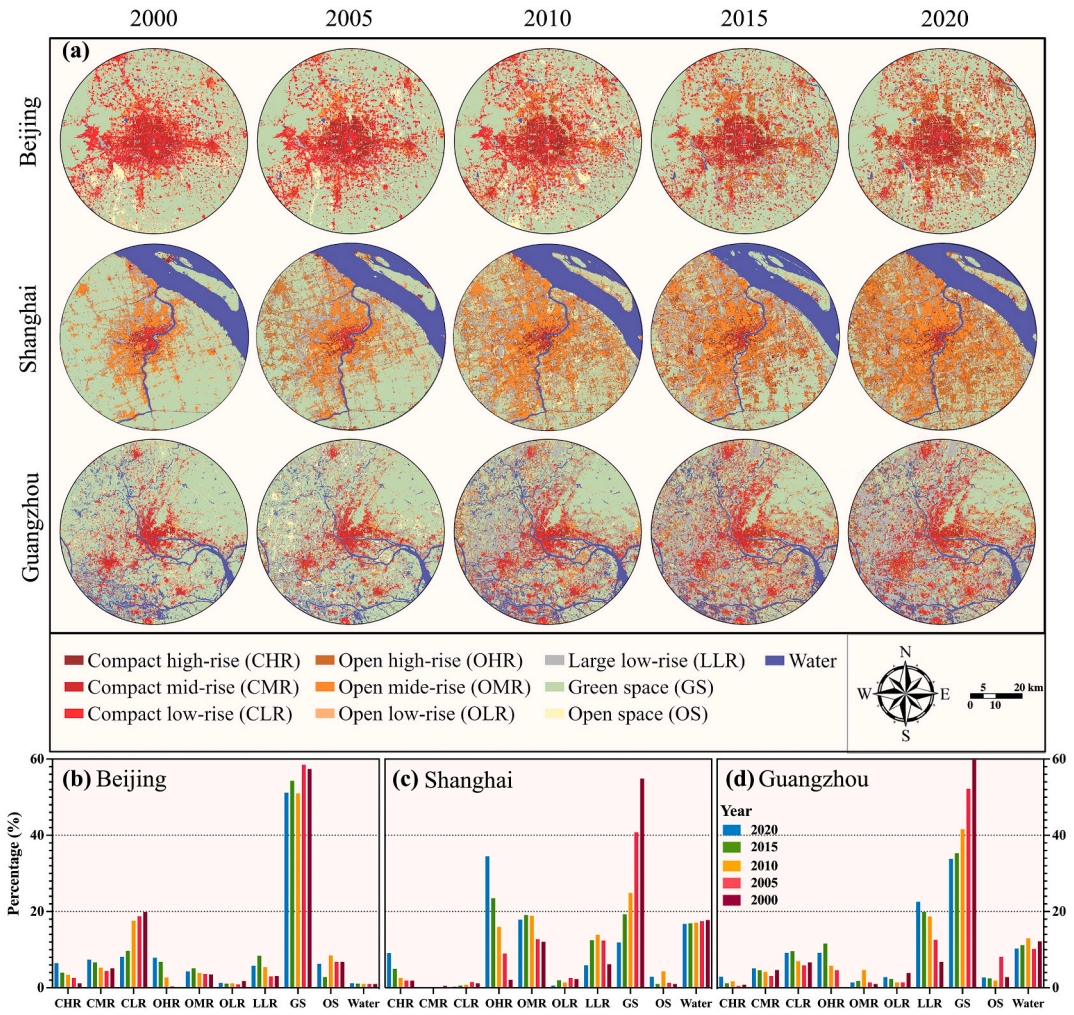


Fig. 6. LCZ maps across different cities and years (a); the percentages of LCZ classes in Beijing (b), Shanghai (c), and Guangzhou (d) in different years.

that the cities varied in their expansion characteristics, especially in the early years of the study period. However, these differences disappeared as cities expanded with OHR and LLR classes in recent years. For example, GS was mainly replaced by the CLR class before 2010 and then transformed to the OHR and LLR classes in Beijing (Fig. 9a). In Shanghai, the GS class was mainly transformed to the OHR, OMR, and LLR classes between 2000 and 2010. After 2010, the built-up area expanded with OHR classes (Fig. 9b). In Guangzhou, the city remained in a near-constant transformation model, and the GS class steadily transformed into the OHR and LLR classes from 2000 to 2020 (Fig. 9c).

3.3.2. *Characterization of urban renewal*

Urban renewal or redevelopment was the major transformation characteristic of the built-up areas. The common trend in all of the cities was an intensification of urban construction as the low-rise classes transformed to comparatively high-rise classes. For example, the OMR class transformed to the OHR class, and the CLR class transformed to the CMR or CHR class. These transformations caused the number of CHR classes to continuously increase, with the percentage of CHR increasing from 1.2 % to 6.5 %, 1.9 % to 9.1 %, and 0.8 % to 2.9 % in Beijing, Shanghai and Guangzhou, respectively. The number of OHR classes dramatically increased, especially after 2010, with the percentage of OHRs increasing from 0.7 % to 8 %, 2.1 % to 34.5 %, and 0.1 % to 9.2 % in Beijing, Shanghai and Guangzhou, respectively.

3.3.3. *3D urban morphology transformation model for Chinese megacities*

The expansion and renewal characteristics of the LCZ classes in three Chinese megacities have shared a similar transformation model in recent years (Fig. 10). Where urban areas were expanded with LLR and OHR classes, LLR was replaced by the CLR and OMR classes, OMR was transformed to the OHR class, and certain OHR classes were finally redeveloped as the CHR class. Moreover, CLR was replaced by CMR, and CMR was transformed to the CHR class. In recent years, several other types of urban expansion or transformation have also occurred. For example, CLR was directly transformed to the CHR class. However, such cases only occurred in certain areas near the city center and can be regarded as minor transformations.

4. Discussion

4.1. *Comparison of the spatial distribution of the 3D urban morphology across global megacities*

Cities are diverse, and this diversity is reflected in their dominant LCZ classes (Taubenböck et al., 2020; Zhu et al., 2022). However, cities may also display several common patterns, such as the spatial preference of different LCZ classes in Chinese megacities. To explore whether these rules exist in global megacities, in addition to the case cities here, we selected eight global megacities for comparison (Fig. 1B, Appendix); they cover most types of cities, as Taubenböck et al. (2020) categorized. The results showed that compact classes (e.g., CHR, CMR and CLR) dominate the urban morphology in all city centers, as these LCZ classes have the highest density around the central city area (DIST <10 km). The open classes (e.g., OMR and OLR) or LLR classes generally appear in

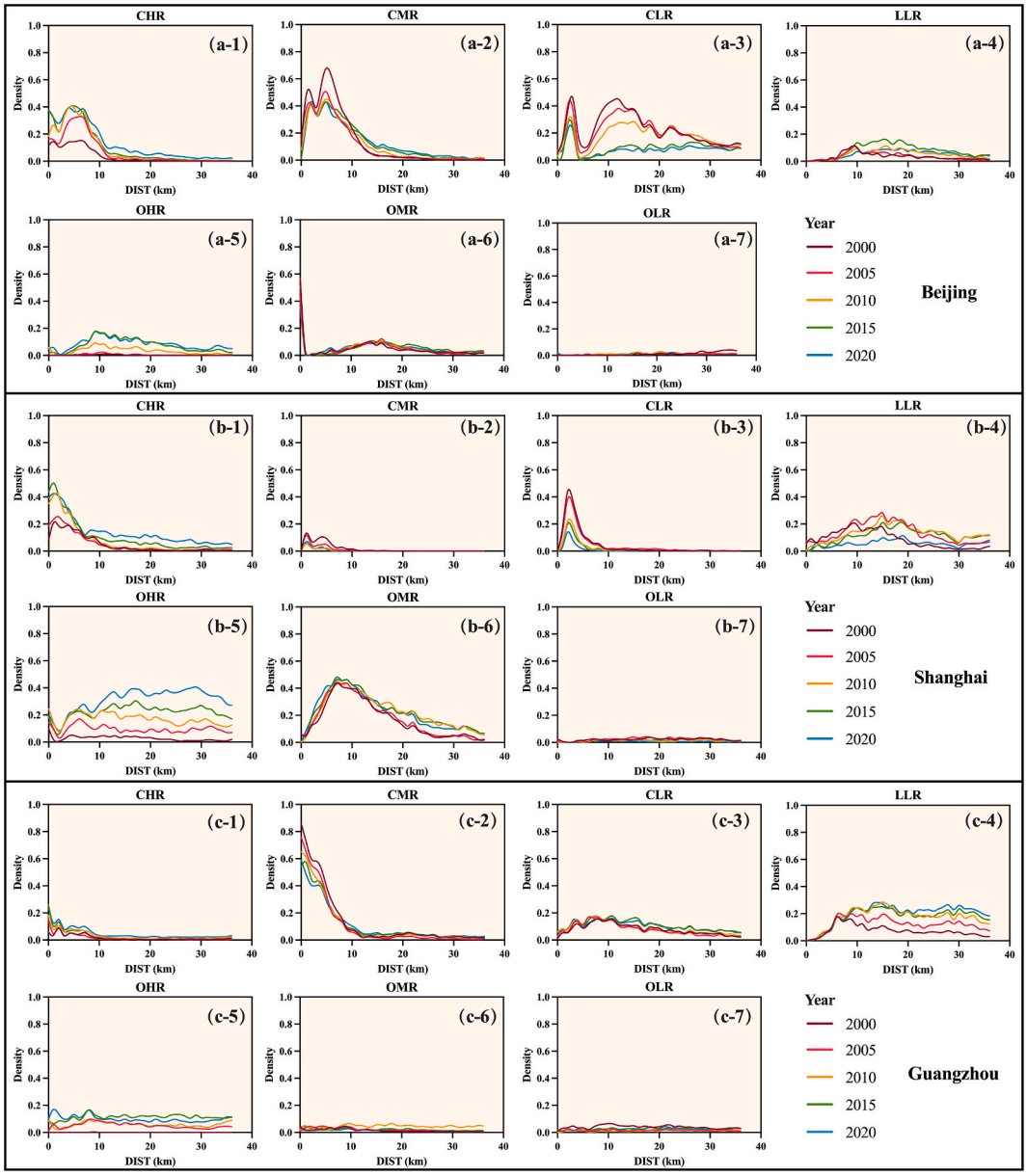


Fig. 7. Spatial distribution of the LCZ density across different cities and years.

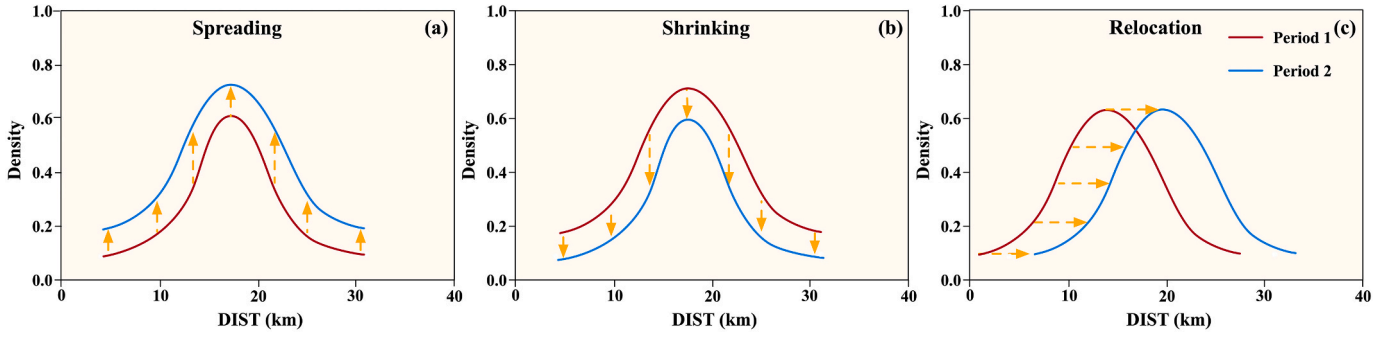


Fig. 8. Three fundamental patterns of the spatial distribution of LCZ classes: spreading (a), shrinking (b) and relocation (c).

suburban areas, with a DIST of approximately 10 km (Fig. 11).

To better understand the characteristics of urban morphology, we select the per capita gross domestic product (GDP) as a critical index that represents cities' economic levels and the stage of urban development. Because the GDP is usually positively correlated with urban development, therefore, present-day cities with different economic levels can be

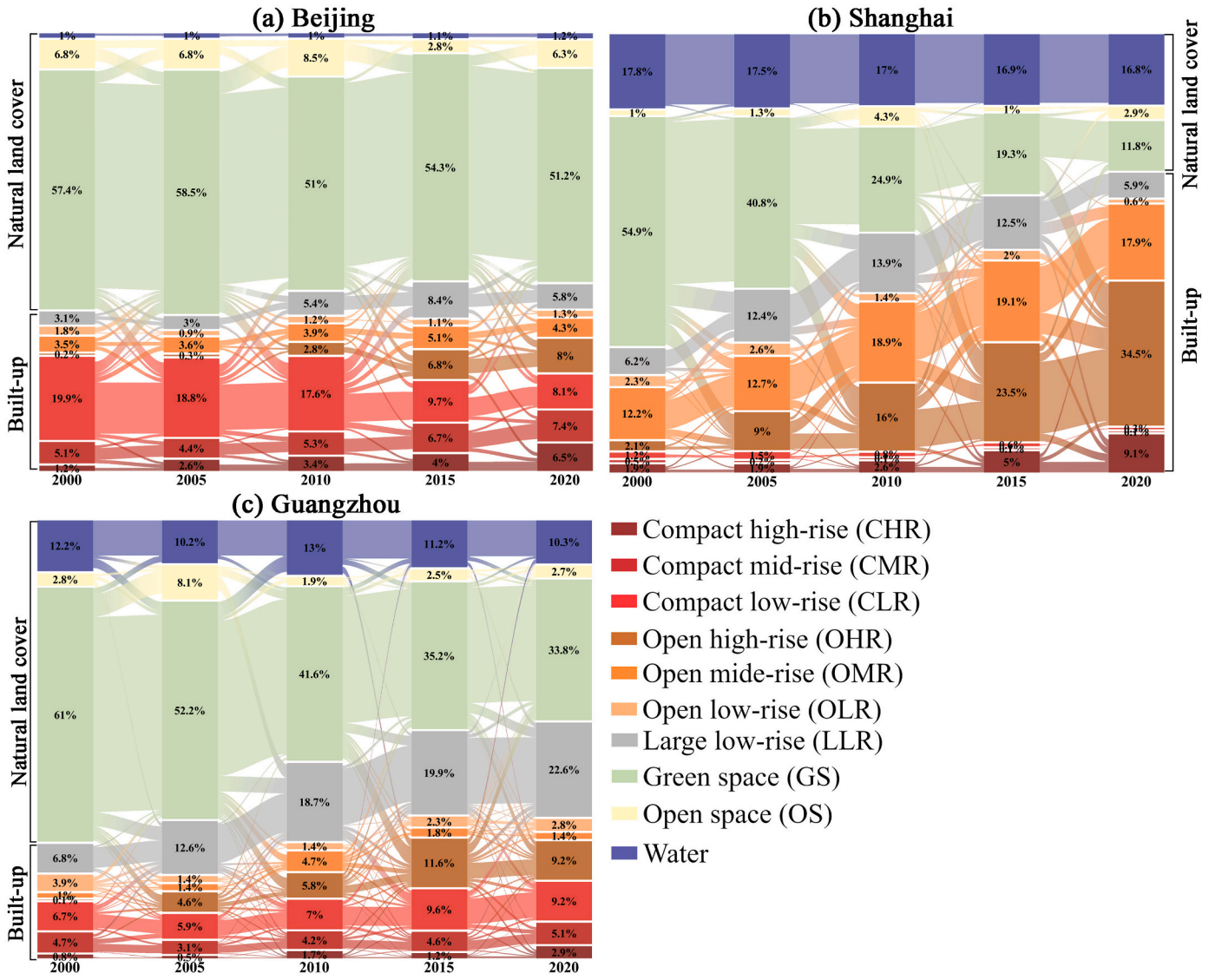


Fig. 9. Alluvial diagram of LCZ classes across different cities and periods.

used to explore the transformation of the urban morphology. Fig. 11 shows that cities are dominated by low-intensity classes (e.g., CLR and OLR) at low GDP values. As the GDP increases, several low-intensity classes (especially CLR) display a shrinking pattern, and the high-intensity classes (e.g., CMR, OHR and OMR) exhibit a spreading pattern. Moreover, relocation can be observed for LLR classes with increasing GDP. The findings for these global megacities can inform the expected development of urban morphology in Chinese or other developing megacities. Notably, the CHR, CMR and OHR classes are increasing, and the CLR class is shrinking.

4.2. *Driving forces of the 3D urban morphology*

Cities are driven by various forces, such as government policies, climate conditions and socioeconomic factors (Long et al., 2012; Wu et al., 2021; Yang et al., 2020). Regarding driving forces, several traditional 2D theories can be applied to explain the characteristics and transformation of the 3D urban morphology. For example, location theory supports the idea that cities are driven by economic activity (Isard, 1956). Notably, the land price decreases with increasing distance to the city center, which leads to intensified land construction and the formation of compact classes in the city center and open and LLR classes distributed in peripheral urban areas.

In addition to economic activity, other forces also drive urban morphology. The population can serve as an example. Population size displayed a significant positive relationship with the urban built-up area, and the Pearson correlations were 0.76** (Beijing), 0.91** (Shanghai) and 0.90** (Guangzhou). These outcomes indicate that population played an active role in promoting urban expansion. However, the spatial distribution of the population did not keep pace with urban expansion. As shown in Fig. 12 urban expansion mainly occurred in suburban or rural areas, because the density of built-up classes in the city center increases at a slower pace than that in suburban or rural areas. In contrast, most city inhabitants live in urban core areas. In these areas, the population density (PD) is increasing faster than that in suburban areas (Fig. 13a). According to the coordination of supply and demand in urban areas, the following relationship can be established:

$$Population \times per\ capita\ spaces = Built\ up\ area \times land\ development\ intensity \quad (2)$$

The preceding equation can be converted into the following form:

$$\frac{Population}{Built\ up\ area} = \frac{land\ development\ intensity}{per\ captia\ spaces} \quad (3)$$

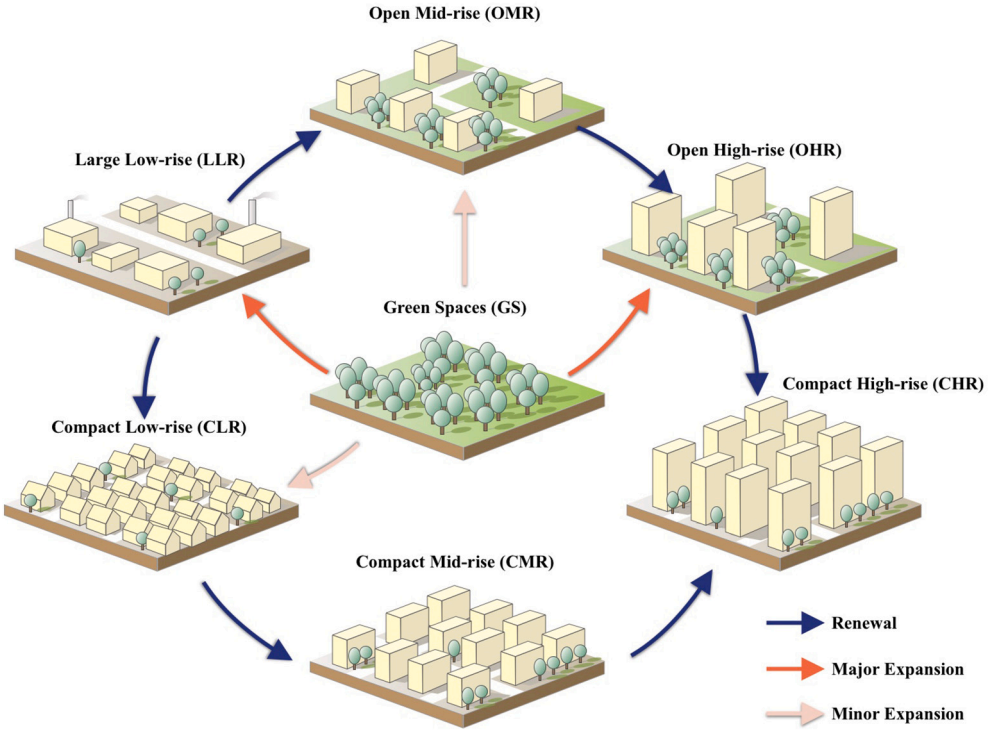


Fig. 10. Urban morphology transformation model for Chinese megacities.

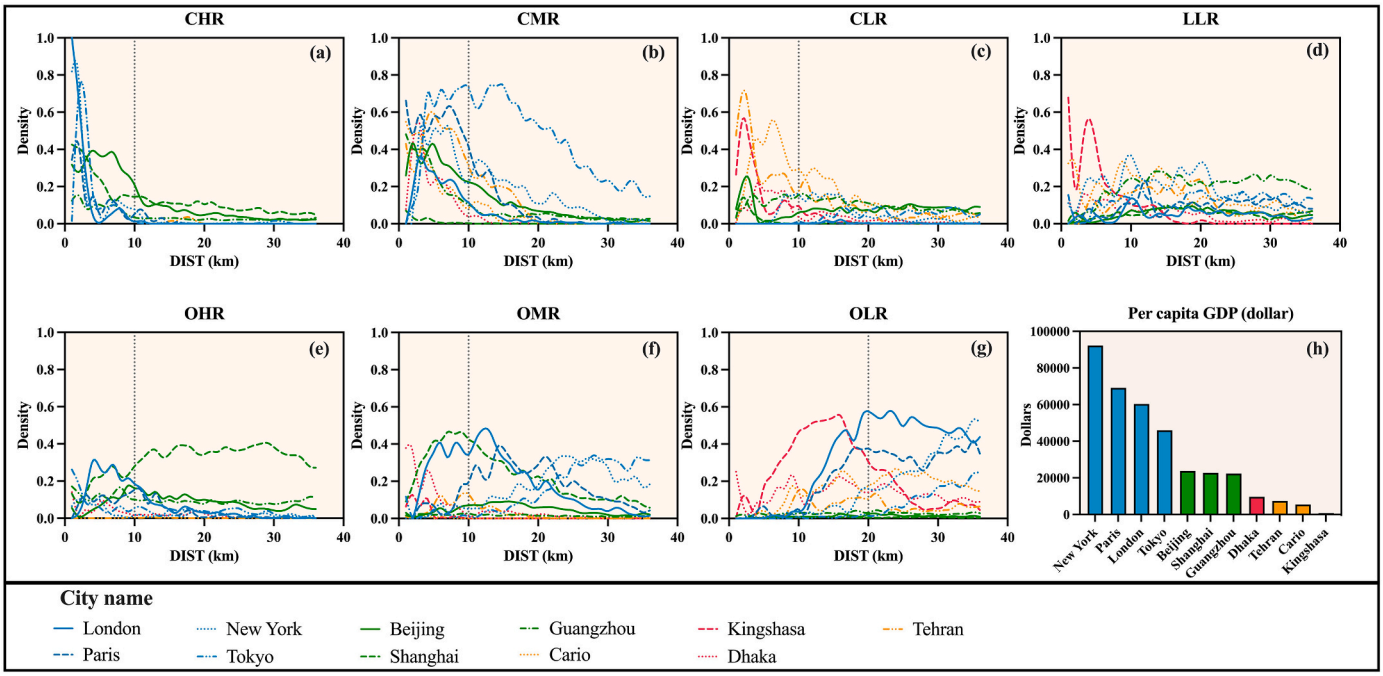


Fig. 11. Spatial distribution of the LCZ density across global megacities for the year around 2020 (a-g) and average GDP in different cities (h).

Therefore, the dislocation development between population growth and built-up areas can produce an uneven distribution of the 3D urban morphology (Fig. 13b). For areas near the city center, population growth was faster than the increase in built-up areas, which can lead to a higher land development intensity or smaller per capita spaces, and produce the formation of compact classes. For areas far from the city center, especially in suburban or rural areas, population growth is often slower than the increase in built-up areas, which can lead to a lower land development intensity or larger per capita spaces and the formation of open or LLR classes.

The imbalance between the growth in population and built-up areas can also impact the dominant LCZ classes across different cities. In Shanghai and Guangzhou, the growth of built-up areas was much faster than their population size (Fig. 13c). In this scenario, residents owned more land spaces (not limited to residential areas), and the cities had to spread in a low-density pattern, producing numerous open or LLR classes. The opposite was true for Beijing, where the growth of built-up areas was slower than their population, leading to the intensified use of

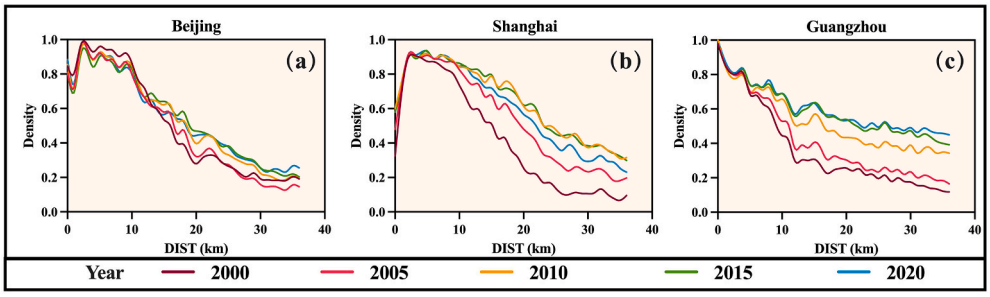


Fig. 12. Spatial distribution of the built-up density across different cities and years.

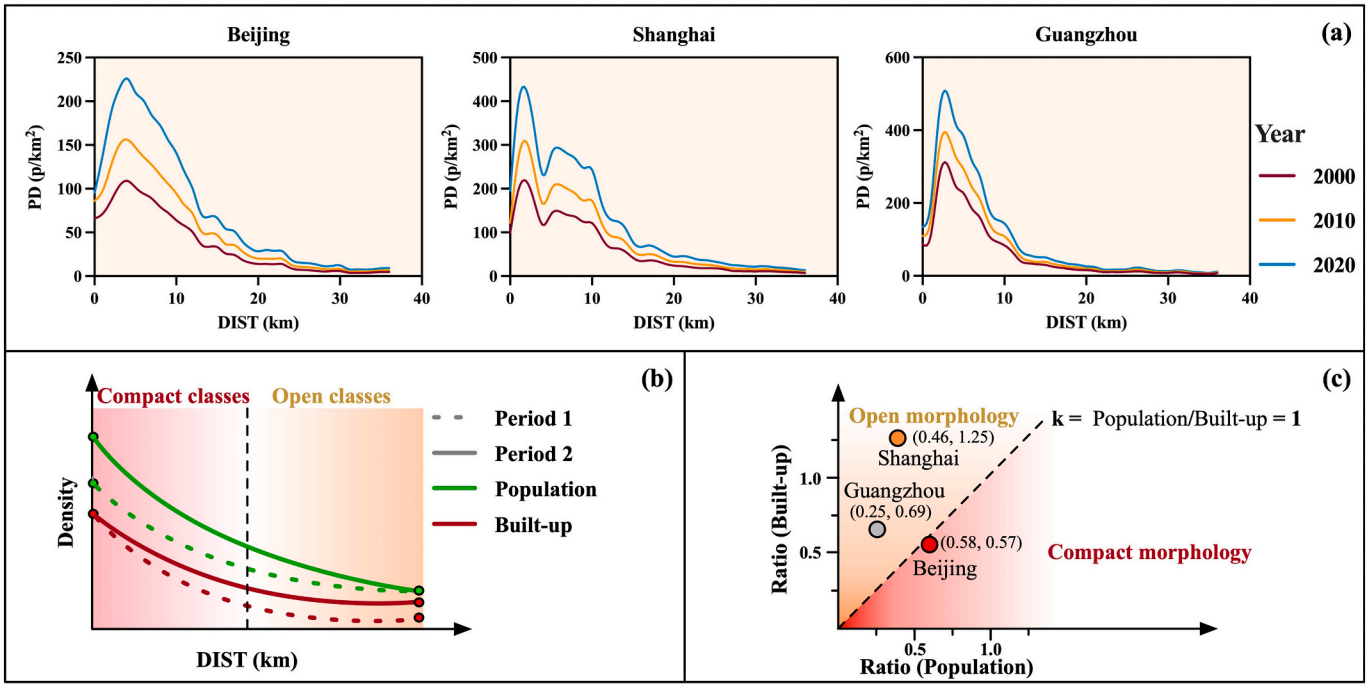


Fig. 13. Spatial distribution of the population density (PD) across different cities and years (a). The dislocation development of population and built-up area can produce an uneven distribution of the 3D urban morphology, as compact classes are distributed in urban core areas and open classes are dominant in suburban areas (b) (this figure is derived from Fig. 12 and Fig. 13a). The imbalanced growth ratio of population and built-up area can produce various dominant LCZ classes across different cities (c).

urban spaces and an urban morphology transformed into compact classes. Therefore, a dense population can accelerate the formation of a compact urban morphology, creating a positive relationship between population density and urban compactness, as has been identified in various global cities (Hu, Wang, Taubenböck, & Zhu, 2021).

Notably, the driving forces of urban morphology are complex and not limited to the economy and population; they also include other forces, such as government controls, transportation developments, information, and communication technology (ICT) transformations (Li et al., 2018; Long et al., 2012; Wu et al., 2021; Zeng, Yu, & Zhang, 2019). These forces combine and interact to influence urban morphology transformations, thus producing nonlinear correlations between driving forces and urban morphology. For example, the relationship between population size, built-up area, and urban morphology is also influenced by economic developments. In Eq. (3), we set per capita space as a constant value that does not change with urban development. In real scenarios, per capita space increases or decreases with economic levels, and is even decoupled from economic activity in some cases. For instance, certain residents can purchase luxury villas under improving financial conditions but cannot afford rent on a small house when incomes worsen. Such forces can distort the coordination relationship between population growth and urban expansion, making the K value in Fig. 13c not equal to 1.

4.3. Policy implications

This study has several implications. First, high spatiotemporal 3D urban morphology maps can expand the data sources of urban studies and provide a database for other issues, such as the urban climate, human health and air pollution. Second, cities are diverse; they vary in their urban landscapes and dominant LCZ classes. However, Chinese megacities also share a common transformation model, making them homogeneous in recent years. Therefore, urban planners and policymakers should consider preserving unique urban landscapes and characteristic areas, such as historical zones. Third, the physical morphology of urban areas, urban functions and human activities are interrelated. For example, the CHR class appears in city center areas and mainly serves office and commercial functions, while the OHR class is generally distributed in suburbs and serves residential functions (Cai et al., 2021); this finding implies that a jobs-housing imbalance will be more serious under the heterogeneous development of urban 3D morphology. Therefore, corresponding methods should be proposed to improve the

connectivity between jobs and housing and address issues such as traffic congestion and energy use. A mix of various urban land uses and urban morphology should also be encouraged. Fourth, the spatial distribution and preferences regarding different LCZ classes can provide examples for planners managing urban land use, controlling the land construction intensity and optimizing the 3D urban morphology. Last, because the driving forces of the 3D urban morphology are complex and vary across different cities, in addition to common actions or rules, the government should introduce comprehensive construction and renewal institutions to support local development, especially during the urban renewal period.

4.4. Limitations and future studies

This study has several limitations. First, there are data limitations. We used satellite images to label training samples and classify urban morphology. This approach depends on the optical characteristics of buildings, such as shadows, from which the surface area or height of buildings are identified and calculated. If buildings are densely distributed or directly adjacent with little open space between them, it is difficult to extract building properties. In addition, buildings with no surface area changes can continue to increase in height, and it is difficult to distinguish such differences. A typical example is the CLR class in Guangzhou city, for which the average number of floors was less than three in approximately 2000, while the average number of floors is currently 6 or greater. Therefore, it is necessary to combine remote sensing images with other data (e.g., LiDAR and RaDAR) or to conduct in situ assessments to improve the LCZ classification accuracy (Zhu et al., 2019). A second shortcoming is associated with the methodology applied. We applied machine learning to identify urban morphology, and the overall accuracy was approximately 0.6 and varied across different cities, even for LCZ classes. For the classes with single land covers, such as water, the accuracy was over 0.9, whereas for classes with complex morphologies, it was approximately 0.5. Although these accuracy levels are sufficient for conducting mesoscale studies, its uncertainty remains and requires improvement. Moreover, we adopted the LCZ scheme and classified 3D urban morphology into 10 classes, which cannot capture the full image of cities. Notably, certain landscape characteristics were simplified. For example, super high-rise buildings were grouped into the CHR class, and areas being demolished or that were previously demolished were grouped into the OS class. Considering more 3D parameters and expanding the number of classes could enhance the extraction of 3D urban information. Third, the time series used was short, and the study context was limited to China. Our study year began in 2000 because no super high spatial-resolution images from before 2000 were available on Google Earth. In future studies, starting analyses in 1985 or even earlier would be more interesting since Chinese economic reform began in 1987 and urbanization accelerated after 1990. In subsequent years, the Chinese mainland experienced vast urban landscape changes. Thus, a long time series could capture the full process of Chinese urbanization. A solution would be to use deep learning to retrieve super-high-resolution images based on Landsat images and then use these data to establish samples to train models and classify the urban morphology (Chen, Li, & Jin, 2021). In addition, we conducted this study in the Chinese context and found that the assessed cities varied in terms of their dominant LCZ classes. Considering the diverse power of driving forces (e.g., climate conditions, cultural factors and economic levels), it would be interesting to conduct comparison studies of more cities across the globe in the future.

5. Conclusions

This study explored the spatial distribution, transformation, and driving forces of the 3D urban morphology in three Chinese megacities based on an adapted LCZ scheme. The results revealed that cities are diverse, and this diversity is reflected in the dominant LCZ classes and spatial distributions. In addition to these diverse characteristics, several common patterns and rules were observed. First, the spatial distribution of different LCZ classes indicates that they follow a density gradient, whereby compact classes were more likely to appear in city centers and open classes were nearly always distributed in suburban areas. The spatial distribution of the LCZ classes dynamically reflected urban development, and the density gradient transformation displayed three fundamental patterns: spreading, shrinking, and relocation. Second, two types of urban morphology transformation were observed: expansion and renewal. In recent years, Chinese megacities have mainly expanded with OHR and LLR classes in rural areas and have been renewed from low-rise to high-rise classes in built-up areas. Finally, urban morphology is driven by multiple forces, such as economic activity and population growth. These forces interact to produce diverse 3D urban morphologies across different cities.

The findings of this paper can help us better understand the mechanisms of 3D urban morphology dynamics as well as the corresponding driving forces. Additionally, the detail and high spatiotemporal resolution of LCZ maps are excellent, and these maps can be used to study urban issues from a 3D perspective. Notably, time series of human health, urban climate and urban renewal issues can be considered in this mapping approach. Such information can help urban planners and policymakers ameliorate urban problems, improve the urban environment, and build livable and sustainable cities.

CRediT authorship contribution statement

Zhi Cai: Conceptualization, Methodology, Writing, Original draft preparation, Visualization. Matthias Demuzere: Methodology, Data curation, Validation. Yan Tang: Supervision, Validation, Funding acquisition, Reviewing. Yongman Wan: Investigation, Data curation.

Declaration of competing interest

The authors declared that they have no conflicts of interest to this work.

Data availability

Data will be made available on request.

Acknowledgments

This work was supported by the National Natural Science Foundation of China (Grant No. 51978363), Beijing Social Science Foundation (Grant No. 19GLB034) and National Key Research and Development Program of China (Grant No. 2018YFC0704600), Beijing Key Laboratory of Spatial Development for Capital Region (Grant No. CLAB202009), Tsinghua × Tencent WeSpace Future Urban Space Funding 2020 (041504196), M. Demuzere is supported by the ENLIGHT project, funded by the German Research Foundation (DFG) under Grant No. 437467569.

Appendix A

Table 1A
Values of different urban canopy parameters for LCZ classes (adapted from Stewart and Oke, 2012).

Adapted LCZ	Original LCZ	Sky view factor	Aspect ratio	Building surface fraction	Impervious surface fraction	Pervious surface fraction	Height of roughness elements (m)	Terrain roughness class	Surface albedo
CHR	LCZ 1 compact high-rise (CHR)	0.2–0.4	> 2	0.4–0.6	o.4–0.6	< 0.1	> 25	8	0.10–0.20
CMR	LCZ 2 compact mid-rise (CMR)	0.3–0.6	0.75–2	0.4–0.7	0.3–0.5	< 0.2	10–25	6–7	0.10–0.20
CLR	LCZ 3 compact low-rise (CLR)	0.2–0.6	0.75–1.5	0.4–0.7	0.2–0.5	< 0.3	3–10	6	0.10–0.20
OHR	LCZ 4 open high-rise (OHR)	0.5–0.7	0.75–1.25	0.2–0.4	0.3–0.4	0.3–0.4	> 25	7–8	0.12–0.25
OMR	LCZ 5 open mid-rise (OMR)	0.5–0.8	0.3–0.75	0.2–0.4	0.3–0.5	0.2–0.4	10–25	5–6	0.12–0.25
OLR	LCZ 6 open low-rise (OLR)	0.6–0.9	0.3–0.75	0.2–0.4	0.2–0. 5	0.3–0.6	3–10	5–6	0.12–0.25
None	LCZ 7 lightweight low-rise	0.2–0.5	1–2	0.6–0.9	< 0.2	< 0.3	2–4	4–5	0.15–0.35
LLR	LCZ 8 large low-rise (LLR)	> 0.7	0.1–0.3	0.1–0.2	0.4–0.5	< 0.2	3–10	5	0.15–0.25
OLR	LCZ 9 sparsely built (SB)	> 0.8	0.1–0.25	0.2–0.3	< 0.2	0.6–0.8	3–10	5–6	0.12–0.25
LLR	LCZ 10 heavy industry (HI)	0.6–0.9	0.2–0.5	< 0.1	0.2–0.4	0.4–0.5	5–15	5–6	0.12–0.20
Green space (GS)	LCZ A dense trees	< 0.4	> 1	< 0.1	< 0.1	> 0.9	3–30	8	0.10–0.20
Green spaces (GS)	LCZ B scattered trees	0.5–0.8	0.25–0.75	< 0.1	< 0.1	> 0.9	3–15	5–6	0.15–0.25
Green spaces (GS)	LCZ C bush, scrub	0.7–0.9	0.25–1.0	< 0.1	< 0.1	> 0.9	< 2	4–5	0.15–0.25
Green space (GS)	LCZ D low plants	> 0.9	< 0.1	< 0.1	< 0.1	> 0.9	< 1	3–4	0.15–0.30
Open space (OS)	LCZ E bare rock or paved	> 0.9	< 0.1	< 0.1	> 0.9	< 0.1	< 0.25	1–2	0.20–0.35
Open space (OS)	LCZ F bare soil or sand	> 0.9	< 0.1	< 0.1	< 0.1	> 0.9	< 0.25	1–2	0.20–0.35
Water	LCZ G water	> 0.9	< 0.1	< 0.1	< 0.1	> 0.9	–	1	0.02–0.10

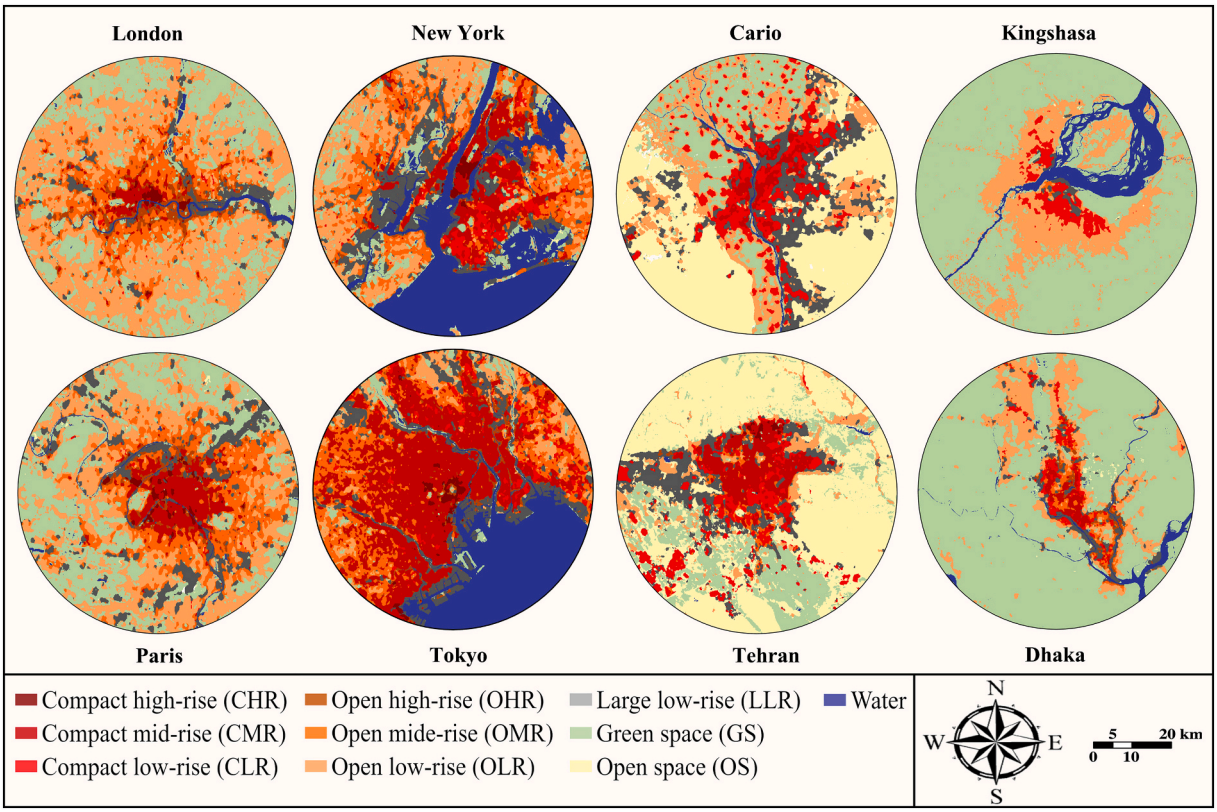


Fig. 1B. LCZ maps across different cities in 2018 (adapted from Demuzere, Kittner, Martilli, et al., 2022).

References

Bechtel, B., Alexander, P. J., Böhner, J., Ching, J., Conrad, O., Feddema, J.Stewart, I., … (2015). Mapping local climate zones for a worldwide database of the form and function of cities. *ISPRS International Journal of Geo-Information, 4*(1), 199–219.

Bechtel, B., Alexander, P. J., Beck, C., Böhner, J., Brousse, O., Ching, J.Xu, Y., … (2019). Generating WUDAPT level 0 data–Current status of production and evaluation. *Urban Climate, 27*, 24–45.

Bechtel, B., Demuzere, M., & Stewart, I. D. (2020). A weighted accuracy measure for land cover mapping: Comment on Johnson et al. Local Climate Zone (LCZ) Map Accuracy Assessments Should Account for Land Cover Physical Characteristics that Affect the Local Thermal Environment. Remote Sens. 2019, 11, 2420. *Remote Sensing, 12*(11), 1769.

Biljecki, F., & Ito, K. (2021). Street view imagery in urban analytics and GIS: A review. *Landscape and Urban Planning, 215*, Article 104217.

Brousse, O., Georganos, S., Demuzere, M., Vanhuysse, S., Wouters, H., Wolff, E. Dujardin, S., … (2019). Using local climate zones in sub-Saharan Africa to tackle urban health issues. *Urban Climate, 27*, 227–242.

Cai, Z., Han, G., & Chen, M. (2018). Do water bodies play an important role in the relationship between urban form and land surface temperature? *Sustainable Cities and Society, 39*, 487–498.

Cai, Z., Tang, Y., Chen, K., & Han, G. (2019). Assessing the heat vulnerability of different local climate zones in the old areas of a Chinese megacity. *Sustainability, 11*(7), 2032.

Cai, Z., Tang, Y., & Zhan, Q. (2021). A cooled city? Comparing human activity changes on the impact of urban thermal environment before and after city-wide lockdown. *Building and Environment, 195*, Article 107729.

Cao, Z., Wu, Z., Liu, L., Chen, Y., & Zou, Y. (2019). Assessing the relationship between anthropogenic heat release warming and building characteristics in Guangzhou: A sustainable development perspective. *Science of the Total Environment, 695*, Article 133759.

Cao, Q., Luan, Q., Liu, Y., & Wang, R. (2021). The effects of 2D and 3D building morphology on urban environments: A multi-scale analysis in the Beijing metropolitan region. *Building and Environment, 192*, Article 107635.

Carmon, N. (1999). Three generations of urban renewal policies: Analysis and policy implications. *Geoforum, 30*(2), 145–158.

Chen, F. (2014). *Urban morphology and citizens' life*.

Chen, B., Li, J., & Jin, Y. (2021). Deep learning for feature-level data fusion: Higher resolution reconstruction of historical Landsat archive. *Remote Sensing, 13*(2), 167.

Ching, J., Mills, G., Bechtel, B., See, L., Feddema, J., Wang, X.Theeuwes, N., … (2018). WUDAPT: An urban weather, climate, and environmental modeling infrastructure for the Anthropocene. *Bulletin of the American Meteorological Society, 99*(9), 1907–1924.

<collab>NBS, N. B.o. S. (2020). Available at https://data.stats.gov.cn/easyquery.htm?cn=C01.

Cox, W. (2021). *Demographia world urban areas [R]* (17th Annual ed.).

Demuzere, M., Bechtel, B., & Mills, G. (2019a). Global transferability of local climate zone models. *Urban Climate, 27*, 46–63.

Demuzere, M., Bechtel, B., Middel, A., & Mills, G. (2019b). Mapping Europe into local climate zones. *PloS one, 14*(4), Article e0214474.

Demuzere, M., Hankey, S., Mills, G., Zhang, W., Lu, T., & Bechtel, B. (2020a). Combining expert and crowd-sourced training data to map urban form and functions for the continental US. *Scientific Data, 7*(1), 1–13.

Demuzere, M., Mihara, T., Redivo, C. P., Feddema, J., & Setton, E. (2020). *Multi-temporal LCZ maps for Canadian functional urban areas*.

Demuzere, M., Kittner, J., & Bechtel, B. (2021). LCZ generator: A web application to create local climate zone maps. In *Frontiers in Environmental Science*.

Demuzere, M., Kittner, J., Martilli, A., et al. (2022). A global map of local climate zones to support earth system modelling and urban-scale environmental science. *Earth System Science Data, 14*(8), 3835–3873. https://doi.org/10.5194/essd-14-3835-2022

Du, S., Liu, B., & Zhang, X. (2021). Mapping large-scale and fine-grained urban functional zones from VHR images using a multi-scale semantic segmentation network and object based approach. *Remote Sensing of Environment, 261*, Article 112480.

Fonte, C. C., Lopes, P., See, L., & Bechtel, B. (2019). Using OpenStreetMap (OSM) to enhance the classification of local climate zones in the framework of WUDAPT. *Urban Climate, 28*, Article 100456.

Gaubatz, P. (1995). Changing Beijing. *Geographical Review*, 79–96.

Gaubatz, P. (1999). China's urban transformation: patterns and processes of morphological change in Beijing, Shanghai and Guangzhou. *Urban Studies, 36*(9), 1495–1521.

Geiß, C., Schrade, H., Pelizari, P. A., & Taubenböck, H. (2020). Multistrategy ensemble regression for mapping of built-up density and height with Sentinel-2 data. *ISPRS Journal of Photogrammetry and Remote Sensing, 170*, 57–71.

Grekousis, G. (2019). Artificial neural networks and deep learning in urban geography: A systematic review and meta-analysis. *Computers, Environment and Urban Systems, 74*, 244–256.

Hatvani-Kovacs, G., Bush, J., Sharifi, E., & Boland, J. (2018). Policy recommendations to increase urban heat stress resilience. *Urban Climate, 25*, 51–63.

He, Q., Zeng, C., Xie, P., Tan, S., & Wu, J. (2019). Comparison of urban growth patterns and changes between three urban agglomerations in China and three metropolises in the USA from 1995 to 2015. *Sustainable Cities and Society, 50*, Article 101649.

Hu, J., Wang, Y., Taubenböck, H., & Zhu, X. X. (2021). Land consumption in cities: A comparative study across the globe. *Cities, 113*, Article 103163.
Isard, W. (1956). *Location and space-economy*.
Jiang, S., Huang, F., Zhan, W., Bechtel, B., Liu, Z., Demuzere, M., & Zhang, X. (2021). *Mapping local climate zones: A bibliometric meta-analysis and systematic review*.
Jiao, L. (2015). Urban land density function: A new method to characterize urban expansion. *Landscape and Urban Planning, 139*, 26–39.
Kovács, Z., Farkas, Z. J., Egedy, T., Kondor, A. C., Szabó, B., Lennert, J.Kohán, B., … (2019). Urban sprawl and land conversion in post-socialist cities: The case of metropolitan Budapest. *Cities, 92*, 71–81.
LeCun, Y., Bengio, Y., & Hinton, G. (2015). Deep learning. *Nature, 521*(7553), 436–444.
Lee, L. O. F., & Li, O. (1999). *Shanghai modern: The flowering of a new urban culture in China, 1930–1945*. Harvard University Press.
Lemoine-Rodríguez, R., Inostroza, L., & Zepp, H. (2020). The global homogenization of urban form. An assessment of 194 cities across time. *Landscape and Urban Planning, 204*, Article 103949.
Li, G., Sun, S., & Fang, C. (2018). The varying driving forces of urban expansion in China: Insights from a spatial-temporal analysis. *Landscape and Urban Planning, 174*, 63–77.
Li, W., Liu, H., Wang, Y., Li, Z., Jia, Y., & Gui, G. (2019). Deep learning-based classification methods for remote sensing images in urban built-up areas. *IEEE Access, 7*, 36274–36284.
Li, M., Koks, E., Taubenböck, H., & van Vliet, J. (2020). Continental-scale mapping and analysis of 3D building structure. *Remote Sensing of Environment, 245*, Article 111859.
Li, H., Liu, Y., Zhang, H., Xue, B., & Li, W. (2021). Urban morphology in China: Dataset development and spatial pattern characterization. *Sustainable Cities and Society, 71*, Article 102981.
Long, Y., Gu, Y., & Han, H. (2012). Spatiotemporal heterogeneity of urban planning implementation effectiveness: Evidence from five urban master plans of Beijing. *Landscape and Urban Planning, 108*(2–4), 103–111.
Ma, L., Liu, Y., Zhang, X., Ye, Y., Yin, G., & Johnson, B. A. (2019). Deep learning in remote sensing applications: A meta-analysis and review. *ISPRS Journal of Photogrammetry and Remote Sensing, 152*, 166–177.
Mabon, L., Kondo, K., Kanekiyo, H., Hayabuchi, Y., & Yamaguchi, A. (2019). Fukuoka: Adapting to climate change through urban green space and the built environment? *Cities, 93*, 273–285.
Meng, L., Sun, Y., & Zhao, S. (2020). Comparing the spatial and temporal dynamics of urban expansion in Guangzhou and Shenzhen from 1975 to 2015: A case study of pioneer cities in China's rapid urbanization. *Land Use Policy, 97*, Article 104753.
Middel, A., Nazarian, N., Demuzere, M., & Bechtel, B. (2022). Urban climate informatics: An emerging research field. *Frontiers in EnvironmentalScience, 532*.
Milojevic-Dupont, N., & Creutzig, F. (2020). Machine learning for geographically differentiated climate change mitigation in urban areas. *Sustainable Cities and Society, 64*, Article 102526.
Potgieter, J., Nazarian, N., Lipson, M. J., Hart, M. A., Ulpiani, G., Morrison, W., & Benjamin, K. (2021). Combining high-resolution land use data with crowdsourced air temperature to investigate intra-urban microclimate. *Frontiers in EnvironmentalScience, 385*.
Ren, C., Cai, M., Li, X., Zhang, L., Wang, R., Xu, Y., & Ng, E. (2019). Assessment of local climate zone classification maps of cities in China and feasible refinements. *Scientific Reports, 9*(1), 1–11.
Rosvall, M., & Bergstrom, C. T. (2010). Mapping change in large networks. *PloS one, 5*(1), Article e8694.
Stewart, I. D., & Oke, T. R. (2012). Local climate zones for urban temperature studies. *Bulletin of the American Meteorological Society, 93*(12), 1879–1900.
Taubenböck, H., Esch, T., Felbier, A., Wiesner, M., Roth, A., & Dech, S. (2012). Monitoring urbanization in mega cities from space. *Remote Sensing of Environment, 117*, 162–176.
Taubenböck, H., Standfuß, I., Wurm, M., Krehl, A., & Siedentop, S. (2017). Measuring morphological polycentricity-A comparative analysis of urban mass concentrations using remote sensing data. *Computers, Environment and Urban Systems, 64*, 42–56.
Taubenböck, H., Debray, H., Qiu, C., Schmitt, M., Wang, Y., & Zhu, X. X. (2020). Seven city types representing morphologic configurations of cities across the globe. *Cities, 105*, Article 102814.
Vandamme, S., Demuzere, M., Verdonck, M. L., Zhang, Z., & Van Coillie, F. (2019). Revealing Kunming's (China) historical urban planning policies through local climate zones. *Remote Sensing, 11*(14), 1731.
Wang, R., Cai, M., Ren, C., Bechtel, B., Xu, Y., & Ng, E. (2019). Detecting multi-temporal land cover change and land surface temperature in Pearl River Delta by adopting local climate zone. *Urban Climate, 28*, Article 100455.
Wentz, E. A., York, A. M., Alberti, M., Conrow, L., Fischer, H., Inostroza, L. Taubenböck, H., … (2018). Six fundamental aspects for conceptualizing multidimensional urban form: A spatial mapping perspective. *Landscape and Urban Planning, 179*, 55–62.
Wu, F. (2015). *Planning for growth: Urban and regional planning in China*. Routledge.
Wu, R., Li, Z., & Wang, S. (2021). The varying driving forces of urban land expansion in China: Insights from a spatial-temporal analysis. *Science of the Total Environment, 766*, Article 142591.
Xu, Y., Ren, C., Ma, P., Ho, J., Wang, W., Lau, K. K. L.Ng, E., … (2017). Urban morphology detection and computation for urban climate research. *Landscape and Urban Planning, 167*, 212–224.
Xu, G., Dong, T., Cobbinah, P. B., Jiao, L., Sumari, N. S., Chai, B., & Liu, Y. (2019). Urban expansion and form changes across African cities with a global outlook: Spatiotemporal analysis of urban land densities. *Journal of Cleaner Production, 224*, 802–810.
Yang, R., Zhang, J., Xu, Q., & Luo, X. (2020). Urban-rural spatial transformation process and influences from the perspective of land use: A case study of the Pearl River Delta region. *Habitat International, 104*, Article 102234.
Yu, X. J., & Ng, C. N. (2007). Spatial and temporal dynamics of urban sprawl along two urban–rural transects: A case study of Guangzhou,China. *Landscape and Urban Planning, 79*(1), 96–109.
Yu, X., Wu, X., Luo, C., & Ren, P. (2017). Deep learning in remote sensing scene classification: A data augmentation enhanced convolutional neural network framework. *GIScience & Remote Sensing, 54*(5), 741–758.
Zeng, H., Yu, X., & Zhang, J. (2019). Urban village demolition, migrant workers' rental costs and housing choices: Evidence from Hangzhou, China. *Cities, 94*, 70–79.
Zhang, Q., & Seto, K. C. (2011). Mapping urbanization dynamics at regional and global scales using multi-temporal DMSP/OLS nighttime light data. *Remote Sensing of Environment, 115*(9), 2320–2329.
Zhang, P., Kohli, D., Sun, Q., Zhang, Y., Liu, S., & Sun, D. (2020). Remote sensing modeling of urban density dynamics across 36 major cities in China: Fresh insights from hierarchical urbanized space. *Landscape and Urban Planning, 203*, Article 103896.
Zhao, C., Weng, Q., & Hersperger, A. M. (2020a). Characterizing the 3-D urban morphology transformation to understand urban-form dynamics: A case study of Austin, Texas, USA. *Landscape and Urban Planning, 203*, Article 103881.
Zhao, M., Zhou, Y., Li, X., Cheng, W., Zhou, C., Ma, T.Huang, K., … (2020b). Mapping urban dynamics (1992–2018) in Southeast Asia using consistent nighttime light data from DMSP and VIIRS. *Remote Sensing of Environment, 248*, Article 111980.
Zhu, Z., Zhou, Y., Seto, K. C., Stokes, E. C., Deng, C., Pickett, S. T., & Taubenböck, H. (2019). Understanding an urbanizing planet: Strategic directions for remote sensing. *Remote Sensing of Environment, 228*, 164–182.
Zhu, X. X., Qiu, C., Hu, J., Shi, Y., Wang, Y., Schmitt, M., & Taubenböck, H. (2022). The urban morphology on our planet–Global perspectives from space. *Remote Sensing of Environment, 269*, Article 112794.